Survey for critical raw materials in Malawi East African Rift geothermal areas

(https://doi.org/10.5880/GFZ.DMJQ.2025.001)

Franziska D.H. Wilke[1], Kondwani T. Gondwe[2], Simona Regenspurg[1], Martin Zimmer[1], Bettina Strauch[1], Jessica A. Stammeier[1], Lukas Klose[3], Timmu Kreitsmann[3,4], Michael Bau[3], Samuel Niedermann[1]

1. *GFZ Helmholtz Centre for Geosciences, Potsdam, Germany*
2. *Department of Energy Systems, Mzuzu University, Mzuzu, Malawi*
3. *School of Science, Constructor University, Bremen, Germany*
4. *Department of Geology, University of Tartu, Estonia*

1. Licence

2. Citation

When using the data please cite:

Wilke, F. D. H.; Gondwe, K. T.; Regenspurg, S.; Zimmer, M.; Strauch, B.; Klose, L.; Kreitsmann, T.; Bau, M.; Niedermann, S.; Stammeier, J (2025): Survey of critical raw materials in Malawi East African Rift geothermal areas. GFZ Data Services. https://doi.org/10.5880/GFZ.DMJQ.2025.001

3. Table of contents

4. Geology

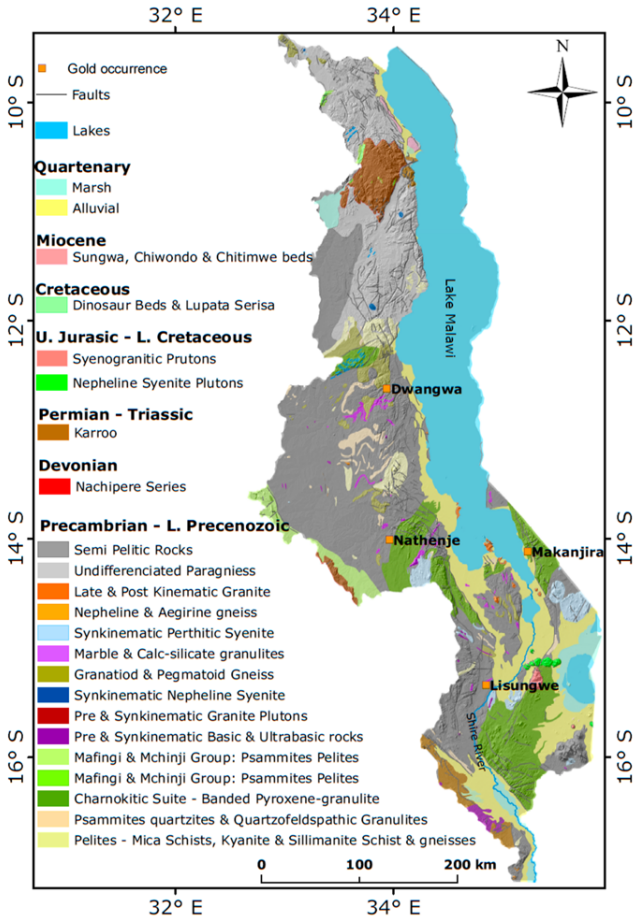

Fig. 1 Geological and structural map of Malawi with lake outlines (after Addison et al., 2020)

The East African Rift System (EARS) continues south of the Afar Crossing in Ethiopia through Kenya and then splits into two branches: the western branch, which runs through Uganda and Rwanda, and the eastern branch, which runs through Tanzania. Both unite in Malawi. Magmatic activity began 20 million years ago south of Lake Turkana (Kenya). Here, destabilisation of the continental lithosphere and extrusion of phonolitic floods occurred, and after a phase of resurgence, small-scale ultra-alkaline, Si-saturated activity took place between ca. 5.9 and 2.9 Ma, defining the early rift development and volcanic initiation phase. Volcanism in the western branch of the EARS is confined to four spatially restricted provinces, all of which are found at the tips of long boundary faults or in accommodation zones between rift segments (Ebinger et al., 1989). The Malawi Rift begins in the southernmost of these volcanic provinces, the Rungwe Volcanic Province (RVP). A slight decrease in mantle velocities is observed below the Malawi Rift, but these velocities are much higher than those below the RVP, suggesting limited magmatism below the Malawi Rift away from the RVP (Schillington et al., 2020). The onset of extension in the Malawi Rift is estimated at 23 Ma (Mortimer et al., 2016) and volcanism in the RVP at 17-24 Ma (Mesko, 2019).

The basement in Malawi is dominated by granites and gneisses sometimes with alkaline geochemistry. In the northern Malawi, Karoo sedimentary rocks are present. Unconsolidated sediments do overly most of the basement. Volcanic extrusives are only present in the most northern and southern edges of Malawi. South of Lake Malawi, the Thombani, Zomba and Mulanje Massifs are alkaline provinces with REE-bearing carbonatites.

5. Expedition outline and funding

In autumn 2023, an expedition to Malawi was undertaken within the framework of the research project “CRM-geothermal”. Within „CRM-geothermal“ we are looking for an environmentally friendly co-production of critical raw materials together with the provision of geothermal energy. In the EARS, high levels of rare earth elements (REE), Sr, Ba and Mg are expected in waters and solids in areas with alkaline volcanic rocks, while other critical elements, including helium, have been sought in other localities. In particular, the eastern branch is the most juvenile sector and has increased geothermal potential related to hot fluids migrating along permeable faults.

Malawi was traversed along the eastern arm of the EARS from north to south to collect gas, water, rock and sediment samples associated with natural hot springs along Lake Malawi and along rivers. On

site, physical and chemical parameters were measured in-situ and documented together with the geology, infrastructure and domestic use of the hot site. Previously, boreholes had only been drilled for drinking water. In Tisola, the 54°C hot water damaged the plastic pipes used, so another borehole had to be drilled. Drilling sites for geothermal water and energy extraction that are already the focus of the authorities, such as Chiweta, Kasitu and Mawira, were visited and gas and water samples were taken. We strongly support the idea of using geothermal water in rural areas and decentralising the energy supply system to make it less prone to disruption. Therefore, sites in the far north (Wurororuror), in the east (Mpyupyu) and in the far south-west (Tisola) were also visited and samples taken. The survey covered 20 sites, from the Rukwa (or Rugwe) Fault in the north to the Shire and Mwanza Rivers in the south (see Fig. 2).

Fig. 2 The map shows sampling locations with yellow and red needles Latter are in the official focus and are the hottest sites.

6. Summary of results

In comparison to southern Tanzania were the noble gas analysis show a mixed crustal-mantle contribution with helium concentrations reaching up to 7 vol% and 3He/4He ratios up to 3.4 Ra, indicating a clear mantle component the noble gas concentrations from Malawi are less spectacular. Still in Manondo (M20) and Nguala (M6), so in the south and the northern of Malawi, respectively, helium concentrations reaching up 1 vol%. In addition, from the hottest spring location Chiweta (78°C) around 1 vol% He was measured having the largest 3He/4He ratio of 2.7 Ra.

Water from hot springs (32-78 °C) were sampled, in agricultural sites, along Lake Malawi and from the dried riverbeds and shorelines. The pH values of the spring waters range from 7.3 to 9.1. Therewith, spring water temperatures are a little elevated in comparison to Tanzania springs. The pH is comparable to Tanzanian waters from neutral to low alkaline. All samples show sodium as major cation, whereas major anions are variable, therefore, different water types are observed. Whereas M1, M2, M3, M5, M9, and M16 are of sodium-carbonate type, samples M6 and M12 are of sodium-sulfate type and M7 is of sodium-chloride type. Sample M13 is of mixed sodium-sulfate-chloride type. Elevated concentrations of sodium, calcium, silica but also lithium, in comparison to other locations, are found in Chiweta (M7) but also in Tisola (M17) and Chipudze (M18). Dissolved REE in hot springs from Malawi are relatively low and range over three orders of magnitude. Highest concentrations of ∑REE were 196 ng/kg in sample M3, whereas, sample M6 had lowest ∑REE content of 1.19 ng/kg

In the northern Malawi geothermal Province from Mupata (M1), Wurororuror (M3), Makenja (M4) and Wungu (M5) granulites, gneiss and mudstones were sampled apart from related sediments which do come up with the hot spring water. Quartz, albite, epidote-allanite and Fe and Fe-Ti-oxide phases do dominate. The sediment in Nguala (M6) at the shore of Lake Malawi is dominated by Fe and Fe-Ti-oxide phases, beside quartz, albite ± epidote and pargasitic amphibole. In Chiweta (M7) the hottest spring occurs in a fault that exhibits fine mudstone with weathered K-feldspar, albite, mica and carbonates and minor apatite and Fe and Fe-Ti-oxide phases. Mtondolo (M8) and Kasitu (or Chiwi, M9)

springs, latter with the second highest spring water temperature and both at the shore of central Lake Malawi, have high-grade metamorphic host rocks with garnets, mica, quartz, K-feldspar, Fe and Fe-Ti-oxide phases but also some minor REE-bearing phosphates (xenotime, monazite, apatite), zircon and uraninite. In Chombo (M10) and Mawira (M11) no samples could be taken but in Lingona (M12) hot fluids fill a basin within an agricultural site bringing sediments up with Ba-Mn-rich mica beside quartz and feldspar. In southern Malawi, Mulosa (M16) in the east and Tisola (M17) in the west come from granitic host rocks containing quartz, K-feldspar and amphibole with minor apatite and Fe and Fe-Ti-oxide phases.

7. Data set and method description

The data are organised in one file listing all samples and subsamples as rows and Tables A1-A6 (described below) as consecutive columns. Table A1 includes an index saying which component (gas, water, solid) of a sample was analysed for what. Table A2 shows the whole rock analyses. A3.1 – A3.6 present the electron microprobe analyses, A4 the water anion, cation and trace element analyses. Table A5 shows the gas geochemistry and A6 the noble gas analyses.

Table A1. Sample Index

Sample ID, sample name = location, date, GPS coordinates, on-site fluid measurements results and notes. The geologic structure of the sampling site is given as well as the host rock type which was sampled at the location and further solids which were sampled. The following part of the table has information if a thin section is available and which analyses were performed at which component of a specific sample.

Table A2. Whole rock geochemistry

Laboratory: Elements and Minerals of the Earth Laboratory (ElMiE Lab, GFZ Helmholtz Centre for Geosciences, Germany)

Major and some minor elements were analysed using X-ray fluorescence (XRF) on fused glass beads. For analysis of major and trace elements fused beads were prepared using dried flux consisting of Lithium tetraborate (66%) and Lithium metaborate (34%; FX-X65-2, Fluxana GmbH & Co. Kg, Germany). Fused beads were measured with an XRF spectrometer (Zetium, Malvern Panalytical, UK) using a Rh tube. Loss on ignition (LOI) was determined by weight difference after fusion. Long term (ca. 2 years) analytical precision is within 5% (1 SD, n=50) for main elements (percent range) and 10% (SD, n=50) for minor elements (mg/kg range); determined on regular analysis of three reference materials BM, GM, TB (basalt, granite, and shale powder, respectively; Zentrales Geologisches Institut ZGI, Germany).

For trace element analysis samples were digested using the four-acid method. process involving hot aqua regia, HF, and HClO4 in PFA beakers (Savillex Corp., USA) using ultrapure reagents. All samples and blanks including acid blanks were diluted or dissolved, respectively with 2 vol.% HNO3 and doped with 1 µl/l In to correct for sensitivity drift. Dilutions were performed online using an auto diluter system (prepFast, Elemental Scientific Inc.). Dissolved samples were quantified using high-resolution inductively coupled plasma mass spectrometry (ICP-MS, ELEMENT XR, Thermo Scientific, USA).

Trace elements, REE and PGE were measured in separate aliquots and separate analytical sessions. Concentrations were each determined by external calibration with a 3-point calibration line using multi-element standards. Acid blanks were measured within the sequence and subtracted online from raw counts. REEs and PGEs were all measured in high mass resolution mode to avoid isobaric interferences, while the remaining trace elements were measured in the lowest mass resolution possible to maintain high sensitivity while avoiding interferences.

Results of samples and reference materials (SCO-1; GSR-4, sandstone powder, National Research Centre of Geoanalysis, China) are presented in table A2 as the average of two replicate analysis on two separate analytical runs. Two samples (**M6**-20230926 M6_sedi, **M9**_1-2023092_M9_beach) and reference material SCO-1 (cody shale powder, U.S.G.S.) were additionally digested using high pressure autoclaves to break down zircon rich samples. The results of these three were further averaged across the two digestion methods, except for the elements that might be affected by incomplete zircon digestion (Zr, Pb, Th, U). For these elements only the average of the autoclave digestion is presented. The relative standard deviation (rsd) between those two methods is generally within 10% for REE, 15% for trace elements, and within 20 % for heavy metals (Cr, Ci, Ni, Cu, Zn).

PGE were only measured in the two samples that were further processed by autoclave digestion. For this analytical run all dilutions and blanks were performed using 2 vol. % HCl. The calibration solution was prepared freshly prior to analysis. A multi element solution distributed by LabKings was used for analytical quality assurance of the measurements. However, no solid reference powder was successfully analyzed to confirm the performance of the digestion methods regarding PGE. Therefore, these results should be regarded as qualitative information only.

Table A3.1 – A3.7. Microprobe (EPMA) analysis

Laboratory: Microprobe Lab (GFZ Helmholtz Centre for Geosciences, Germany)

Analyses of feldspar (A3.1), epidote and allanite (A3.2), garnet (A3.3), mica and amphibole (A3.4), metal oxides (A3.5), carbonates (A3.6) and phosphates (A3.7) were done at operating conditions of 10-20kV and 5-40 nA with a focused beam for stable phases like garnet, but with 2-15 µm beam for e.g., apatite, feldspar, mica and carbonates. Counting times varied between 10 and 30 s on peaks and half of that on background. Synthetic and natural standards were used from international distributors (GEO MK II, MAC, Smithonian Institute). For amphibole and mica, oxygen equivalents of F and Cl were given after the sum of all wt. %. Such equivalents need to be subtracted from the analytical sum. The oxygen equivalent of F is calculated by multiplying moles of F by 0.4211 and 0.255 by moles of Cl. Detection limits (DL) of elements are roughly 0.01-0.02 wt. % (100-200ppm), except REE, Y, U, Pb, Th, Ta and F, which show 0.003-0.07 wt. %. The DL is given on top of each EPMA data table. Iron is given in Fe2+, where needed Fe3+ is stoichiometrically calculated (Fe2+ x 1.1113= Fe3+) and the theoretical water (H2O) content is given after Deer, Howie and Zusman, 2013. Cells with "–" = not determined, empty cells do not apply.

Table A4. Results of hydrochemical analysis

Laboratories: Constructor University, Bremen

Field analysis: the physicochemical parameters pH-value, redox-value, electric conductivity, and temperature were measured with two WTW Multi 3630 IDS meters. Carbonate/bicarbonate was determined by titration (carbonate hardness field test). Due to high carbonate content in some samples, those samples were diluted in the field with deionised water.

Samples in field (each 15 mL) were prepared by filtering (<0.45 µm). Additionally, a total of eleven 1L samples for major and trace elements (including REE) determination were taken unfiltered (M1, M2, M3, M3a, M5, M6, M7, M9, M12, M16). At Constructor University Bremen these samples were filtered through 0.2 µm cellulose acetate membrane filters and aliquots for dissolved anions (F-, Cl-, Br-, SO42-), total alkalinity, pH and electrical conductivity were taken. Subsequently the samples were acidified to pH of 2 with suprapure HCl (Roth, Germany).

Major cations (Ca, K, Mg, Na and Si) in water samples were determined via SpectroCiros Vision ICP-OES in both 0.45 µm and 0.2 µm filtered samples. Limits of quantification were 3.27 mg/kg for Na, 0.96

mg/kg for K, 0.01 mg/kg for Mg, 0.28 mg/kg for Ca, and 0.27 mg/kg for Si determined as ten times standard deviation of the acid blanks. The SLRS-6 river water reference material was measured as a quality control and the difference from published values was typically less than 5%, except Mg which was better than 18%.

To accurately determine the very low contents of dissolved rare earth elements and yttrium in natural waters from Malawi, the samples were processed following a modified method previously described by Bau and Dulski (1996), which was developed by Shabani et al., (1992). Briefly, 1L of filtered and acidified sample was spiked with Tm (50 ppt). Following Tm spike addition, a small aliquot labelled "original" (~25 ml) was taken to monitor Tm recovery, allow for Tm-yield correction as well as for determination of dissolved trace metals (Li, Rb, Sr, Cs, Ba, Pb, U), while the rest of the sample was passed over an exchange columns loaded with a mixture of ethyl-hexylphosphates. To remove the sample matrix, the loaded columns were flushed with 0.01 M HCl, which was followed by an REE elution step with 6 M HCl. The resulting "eluates" were evaporated to incipient dryness twice, before they were finally taken up in a 0.5 M HNO3 solution. Additional information about the method can be found elsewhere (e.g., Bau and Dulski 1996; Schmidt et al. 2019).

Dissolved trace metals (including REY) were measured via ICP-MS (PerkinElmer Elan 6000) following a standard sample-bracketing and Ru, Re, Rh and Bi as internal standard elements. The content of dissolved trace metals (Li, Rb, Sr, Cs, Ba, Pb, U) were determined from sample "originals", whereas REY were measured in "eluates". The Tm-yield of the eluates was between 94% and 101% of the Tm-spike measured in "originals". Analytical quality was monitored by repeated measurement (N=10) of the reference material SLRS-6. Additionally, an eluate of SLRS-6 was processed for REY determination together with the samples. Analytical accuracy for dissolved trace metals Li, Rb, Sr, Cs, Ba, Pb, U was between 97% and 101% of reported values. For dissolved REY, measured concentrations were within 5% of reported values, except for Eu (106%) and Gd (107%). The Tm-yield of the processed eluate from SLRS-6 showed a Tm-yield of 100% and measured REY concentrations were within 5% of reported values, except for Eu (94%), Gd (107%), and Lu (85%).

Total alkalinity was determined following the method described in Giampouras et al. (2019). The content of dissolved anions was measured by ion chromatography (IC 761, MetrohmTM equipped with a Metrosep A Supp 5 - 250/4, MetrohmTM). Analytical quality was monitored by repeated measurement of in-house freshwater and seawater (OSIL) standard with analytical accuracy ranged between 95% to 102% from expected/spiked concentration.

Table A5. Results of gas geochemistry

Laboratories: Gas Geochemistry Lab (GFZ Helmholtz Centre for Geosciences, Germany)

Gas samples were taken using a funnel-and-tube system, in which gas is collected by sampling bubbles in a glass flask initially filled with spring water, with the gas successively replacing the water in the flask. Sampling was completed (i.e., the stopcocks were closed) when the water was completely evacuated, depending on the gas flow.

The chemical composition of gas samples (H2, He, N2, O2, CH4, Ar, CO2) was analysed at the laboratories of the GFZ using an Omnistar (Pfeiffer Vacuum) quadrupole mass spectrometer with closed ion source and a mass range from 1 to 100 amu. Calibration was performed with two certified test gases and air; the relative standard deviation was <10 %.

Appropriate splits of the samples were analysed for noble gas concentrations.

Table A6: Results of noble gas analyses.

Laboratory: Noble Gas Lab (GFZ Helmholtz Centre for Geosciences, Germany)

To remove the reactive gases (e.g. CO2, CO, H2O, N2, H2, O2 and various hydrocarbon compounds), a pipe loop cooled with dry ice, two titanium sponge getters cooled from 750°C to 400°C during the process, one SAES getter with Zr-Al alloy held at room temperature and a second one at 400°C were used. To separate Ar, Kr, Xe from He and Ne, the heavy gases were quantitatively adsorbed to a stainless-steel frit at 50 K in a cryogenic cold head. For part of the samples, this was not possible due to technical problems. Therefore, an activated charcoal finger cooled with liquid nitrogen was used to trap the heavy noble gases; Xe data are not reported for these measurements because no separation from Ar was possible. Helium and neon were trapped at 11 K in another cold head equipped with activated charcoal. The gases were then released at appropriate desorption temperatures and analysed separately in the sequence Ar, Kr+Xe, He, Ne (or Ar+Kr, He, Ne when using the charcoal finger). More details about measurement procedures can be found in Niedermann et al. (1997).

Noble gas concentrations shown in Table A6 have been calculated assuming a total pressure of 1000 mbar in the sampling flasks; their 2σ uncertainties are estimated at ~10-20%. Dashes show values not measured or not meaningful.

8. Acknowledgements

Samples have been collected by Franziska Wilke, Simona Regenspurg, Martin Zimmer and Bettina Strauch during a field campaign in 2023. This expedition has taken place under the umbrella of the European Union funded project “CRM-Geothermal” but was financed with GFZ expedition money (grant X-031-22-01). We would like to warmly thank Hartmut Lieb for rock crushing and sieving, Heike Rothe for assisting in ICP-MS measurements and Enzio Schnabel for assisting in gas isotope measurements. Uwe Dittmann prepared the rock cuttings and polished the thin sections.

9. References

Addison, M. J., Rivett, M. O., Robinson, H., Fraser, A., Miller, A. M., Phiri, P., Mleta, P., & Kalin, R. M. (2020). Fluoride occurrence in the lower East African Rift System, Southern Malawi. In Science of The Total Environment, Vol. 712, p. 136260. https://doi.org/10.1016/j.scitotenv.2019.136260

Bau, M., Dulski, P., (1996). Anthropogenic origin of positive gadolinium anomalies in river waters. In Earth and Planetary Science Letters, Vol. 143, Issues 1–4, pp. 245–255. https://doi.org/10.1016/0012-821X(96)00127-6

Deer, W. A., Howie, R. A., & Zussman, J. (2013). An introduction to the rock-forming minerals. Mineralogical Society of Great Britain and Ireland. https://doi.org/10.1180/DHZ

Ebinger, C. J., Deino, A. L., Drake, R. E., & Tesha, A. L. (1989). Chronology of volcanism and rift basin propagation: Rungwe Volcanic Province, East Africa. Journal of Geophysical Research, Vol. 94(Issue B11), pp. 15,785–15,803. https://doi.org/10.1029/JB094iB11p15785

Giampouras, M., Garrido, C. J., Zwicker, J., Vadillo, I., Smrzka, D., Bach, W., et al. (2019). Geochemistry and mineralogy of serpentinization-driven hyperalkaline springs in the Ronda peridotites. Lithos Vol. 350–351, p. 105215. https://doi.org/10.1016/j.lithos.2019.105215

Mesko, G. T. (2019). Magmatism at the southern end of the East African Rift System: Origin and role during early stage melting (p. 516). New York: Columbia University. PhD-Thesis.

Mortimer, E., Kirstein, L. A., Stuart, F. M., & Strecker, M. R. (2016). Spatio-temporal trends in normal-fault segmentation recorded by lowtemperature thermochronology: Livingstone fault scarp, Malawi Rift, East African Rift System. Earth and Planetary Science Letters, Vol.455, pp.62–72. https://doi.org/10.1016/j.epsl.2016.08.040

Niedermann, S., Bach, W., & Erzinger, J. (1997). Noble gas evidence for a lower mantle component in MORBs from the southern East Pacific Rise: Decoupling of helium and neon isotope systematics. Geochimica et Cosmochimica Acta, Vol. 61, Issue 13, pp. 2697-2715. https://doi.org/10.1016/S0016-7037(97)00102-6

Schmidt, K., Bau, M., Merschel, G., & Tepe, N., (2019). Anthropogenic gadolinium in tap water and in tap water-based beverages from fast-food franchises in six major cities in Germany. Science of The Total Environment, Vol. 687, pp. 1401–1408. https://doi.org/10.1016/j.scitotenv.2019.07.075

Shabani, M.B., Akagi, Tasuku, Masuda, Akimasa, (1992). Preconcentration of trace rareearth elements in seawater by complexation with bis(2-ethylhexyl) hydrogen phosphate and 2-ethylhexyl dihydrogen phosphate adsorbed on a C18 cartridge and determination by inductively coupled plasma mass spectrometry. Analytical Chemistry, Vol.64, Issue 7, pp.737–743. https://doi.org/10.1021/ac00031a008

Shillington, D. J., Scholz, C. A., Chindandali, P. R. N., Gaherty, J. B., Accardo, N. J., Onyango, E., et al. (2020). Controls on rift faulting in the North Basin of the Malawi (Nyasa) Rift, East Africa. Tectonics, Vol.39, Issue 3. https://doi.org/10.1029/2019TC005633